JOURNAL OF GEOPHYSICAL RESEARCH, VOL. 104, NO. C11, PAGES 25,685–25,696, NOVEMBER 15, 1999

Numerical investigation of baroclinic instability in the Gaspé Current using a frontal geostrophic model

M. K. Reszka and G. E. Swaters
Applied Mathematics Institute, University of Alberta, Edmonton, Canada

Abstract. The Gaspé Current, situated in the western Gulf of St. Lawrence, is an intense, buoyancy-driven jet, which is fed by freshwater runoff from the St. Lawrence River. This coastal current is known to exhibit frequent episodes of instability, culminating in backward breaking waves as well as filaments and eddies. We investigate the observed mesoscale variability in a series of numerical simulations, employing a two-layer frontal geostrophic model that focuses on baroclinic dynamics. Unlike previous studies, we allow for large-amplitude variations of the interface depth, with the possibility of outcroppings, as well as two-way coupling of the dynamic pressures in each layer. It is found that the growth rates and length scales associated with the early evolution of disturbances compare favorably with those observed. Moreover, the mesoscale features resulting from highly nonlinear interactions closely resemble those seen in satellite data.

1. Introduction

Freshwater discharge from the St. Lawrence River drives an intense coastal jet, the Gaspé Current, along the Gaspé Peninsula in the province of Quebec in Canada. This area forms the northwestern part of the Gulf of St. Lawrence and will henceforth be referred to as NWG. The NWG is a 200-km long channel, whose width ranges from $\sim$ 50 km at Pointe des Monts to $\sim$ 100 km at the western tip of Anticosti Island. Seasonal variations in the physical properties of the Gaspé Current reflect various environmental factors, most notably the amount of river discharge [*Benoit et al.*, 1985]. However, the current is more or less permanent and undergoes episodes of instability throughout the year [*Mertz and El-Sabh*, 1989].

This instability takes the form of mesoscale waves, meanders, and eddies. At such times the current often spreads or moves offshore. Importantly, the dimensions of the channel are several times greater than the internal Rossby radius for the area ($\sim$ 10 km). The NWG therefore offers us a convenient nearshore environment for the study of highly nonlinear processes involved in mesoscale variability.

The structure of the Gaspé Current has been thoroughly investigated by *Benoit et al.* [1985], *Tang* [1980b], and others, using in situ measurement (as well as remote sensing) techniques. Strong stratification can be observed in the upper 50 m of the water column, due to both salinity and temperature. Isopycnals often have relatively large gradients and can intersect the surface. Between instability events, the main body of the jet extends 15-20 km offshore [*Mertz et al.*, 1988] and has a mean velocity of $\sim$ 60 cm/s [*Tang*, 1980a]. Beyond Pointe des Monts the coastal jet is augmented by the NWG gyre and local velocities of 80-100 cm/s are not uncommon.

A narrow strip of cold water usually marks the offshore edge of the Gaspé Current. The existence of this temperature anomaly, which has been attributed to local upwelling and mixing [*Tang*, 1980b], presents a straightforward way to observe meandering and backward breaking waves in satellite infrared imagery. Weather is often an obstacle in capturing a continuous development of mesoscale features in the NWG using satellite imagery. However, an excellent example of such a time sequence from the summer of 1978 is given by *Tang* [1980a]. In Figure 1 we present drawings of four images derived from a sequence shown by *Tang* [1980a]. For clarity, only the edge of the current (i.e., the frontal outcropping) has been marked. A large amplitude, backward breaking wave and a smaller amplitude wave immediately to the right are visible on August 5. By August 8 the large wave has collapsed and the small wave has grown considerably. Filamentous growths can be seen on August 7 and August 8.

It should be noted that similar behavior has been observed in the Lower St. Lawrence Estuary (LSLE), an area directly east of the NWG [see, e.g., *Mertz et al.* 1988]. The buoyancy-driven jet present in the LSLE will henceforth be referred to as the Gaspé precursor. While the LSLE is not as wide or as deep as the NWG, it will nevertheless be included in our discussion. Our simulations are specifically aimed at modeling the NWG; however, the instability characteristics observed in the estuarine and gulf current fields are similar enough that our results apply to both, at least in a qualitative sense.

When quasi-geostrophic (QG) theory was applied to the Gaspé Current and its precursor [*Mertz et al.*, 1988, 1990], it was found that QG models give reasonable estimates for length scales and initial growth rates of developing instabilities. However, several studies have noted that QG numer-

Copyright 1999 by the American Geophysical Union.

Paper number 1999JC900189.
0148-0227/99/1999JC900189$09.00

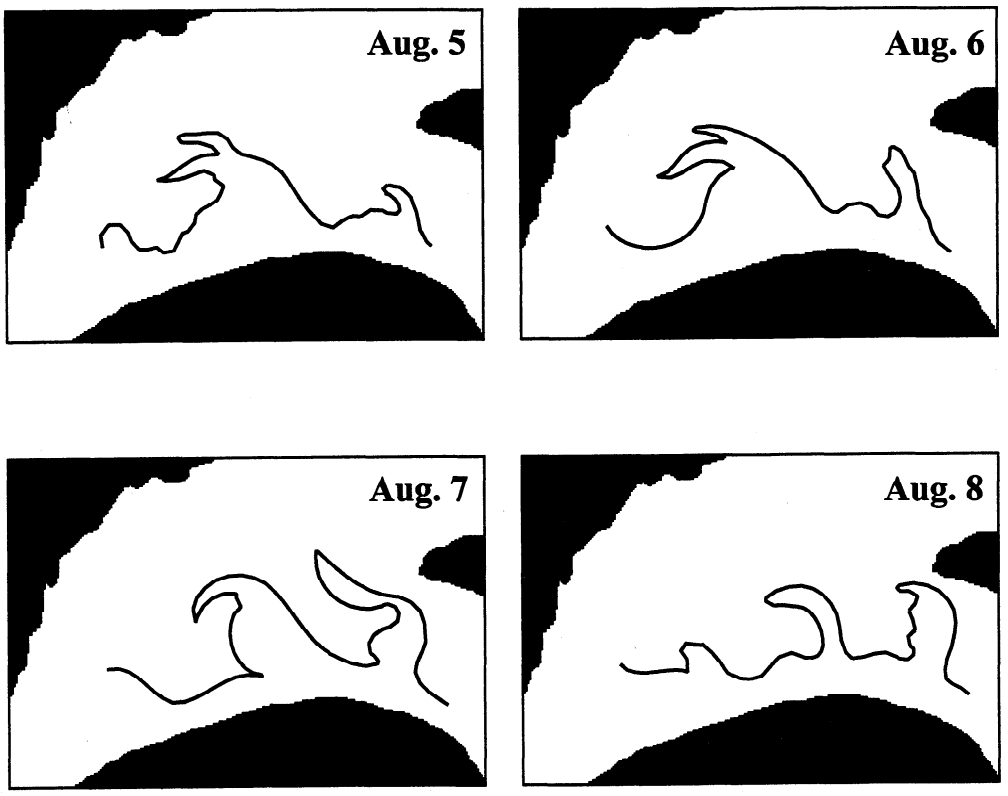

Figure 1. Drawings of an instability episode in the Gaspé Current in August, 1978. Solid line corresponds to the edge of the current, as ascertained from a sequence of satellite images [*Tang*, 1980a].

ical models often cannot accurately predict such quantities [e.g., *Haidvogel et al.*, 1991]. Moreover, the implicit assumption of small isopycnal deflections makes QG theory rather inappropriate for coastal dynamics, where frontal outcroppings are prevalent. In the present work, we employ the two-layer baroclinic frontal geostrophic model derived by *Swaters* [1993] to describe both the early and late stages of frontal evolution in the NWG, in a series of numerical simulations.

The stability characteristics of two monotonically increasing frontal depth profiles are investigated, which qualitatively resemble observations of the Gaspé Current. It is found in both cases that the resulting instability has a dominant wavelength of $\sim$ 60 km and e-folding times of 4-5 days, which compare favorably with observations. Areas of strong cyclonic vorticity develop immediately behind the growing waves, whose crests "break backward" in the terminology of *Griffiths and Linden* [1981]. Further growth of the instability leads to eddy pinch-off and the development of irregular protrusions in the offshore direction. A parameter study involving the bottom topography demonstrates that large cross-channel topographic gradients enhance the instability. In fact, steep bathymetry seems essential in obtaining reasonable growth rates (i.e., comparable to those observed).

The paper is organized as follows. In section 2 we briefly describe the model. In section 3 we provide details concerning the numerical scheme as well as boundary conditions. Section 4 contains the results of simulations employing quadratic and cubic frontal profiles, as well as the parameter study of bottom effects. Detailed comparisons are made with observations of the Gaspé Current and the Gaspé precursor. We present our conclusions in section 5.

2. Governing Equations

Although detailed mathematical derivations of frontal geostrophic models have been fully described for a number of physical configurations, e.g., *Cushman-Roisin* [1986] for a reduced gravity flow on an f plane, *Cushman-Roisin et al.* [1992] for a two-layer flow on a β plane, and independently by *Swaters* [1993] for a two-layer flow over sloping topography (for the underlying noncanonical Hamiltonian structure and general mathematical stability theory, see *Swaters* [1993] and *Karsten and Swaters* [1996]), the underlying dynamical balances assumed in the physics are sufficiently subtle that it is appropriate to review them here. Readers already familiar with the dynamical balances need only to acquaint themselves with our notation as described in our discussion of equations (1) and (2) and may skip directly thereafter to the next section.

Two-layer frontal geostrophic models correspond to a baroclinic subinertial asymptotic limit of the shallow-water equations in which the flow fields are geostrophic to leading order but for which ageostrophic effects are critical to determining the evolution. In the upper layer, these models allow for large-amplitude variations of the upper layer thickness so

that genuine outcroppings can be described. That is, these models do not correspond to a classical QG limit in which the amplitude of the dynamic variations of the interface is small compared to the scale depth of the upper layer. The upper layer mass equation is fully nonlinear and does not reduce to the statement that the flow field is solenoidal to leading order. The dynamic coupling between the two layers, which is rationally accounted for in the model derivation, is nevertheless a second-order effect. Thus, to leading order, the upper layer dynamics are geostrophically degenerate and ageostrophic effects become dynamically important. The evolution of the upper layer geostrophic pressure is determined at second order in the asymptotic expansion by retaining momentum advection and the dynamic coupling between the two layers within the context of a fully nonlinear upper layer mass equation.

Since the local time rate of change of momentum terms is completely neglected in the upper layer, these models filter out Poincaré and Kelvin waves. In addition, the neglect of these terms implies that the upper layer dynamics will not include the local time rate of change of the relative vorticity in the resulting vorticity equation. This occurs because the timescale associated with the dynamics is longer than the advective time scale. As a consequence, the leading order ageostrophic terms in the upper layer momentum equations do not include the time rate of change of momentum terms (but do include momentum and hence vorticity advection and the dynamical coupling between the two layers). The result is a coupled model which retains the advection of relative vorticity while allowing for large-amplitude thickness variations in the upper layer.

The lower layer dynamics is assumed to be QG for which the Eulerian velocity field has been scaled so as to be principally driven by the baroclinic stretching associated with the deforming interface and a background vorticity gradient, i.e., the β effect or variable bottom topography. Because the order of magnitude of the velocity scaling in the lower layer thus determined is smaller than that associated with the upper layer velocity, the local time rate of change terms are the same order of magnitude as the nonlinear advective terms in the momentum equations. Hence the vorticity equation in the lower layer will contain both advective as well as time derivative terms associated with the relative vorticity in contrast to the upper layer vorticity equation. Additionally, of course, the lower layer is dynamically coupled back to the upper layer through baroclinic stretching. From the point of view of the lower layer, the dynamics is "weakly" nonlinear, the upper layer is "thin" compared to the scale depth of the lower layer (as is the amplitude of the dynamic deflections of the interface between the two layers), and the topography is "gently" sloping.

The baroclinic frontal geostrophic model can be derived from the nondimensional, two-layer, rigid-lid, shallow-water equations written in the form

$$\sqrt{\delta}\left(\sqrt{\delta}\partial_t + \mathbf{u}_1\cdot\nabla\right)\mathbf{u}_1 + \mathbf{e}_3\times\mathbf{u}_1 = -\nabla p_1,$$

$$\sqrt{\delta}h_t + \nabla\cdot(\mathbf{u}_1 h) = 0,$$

$$\delta\left(\partial_t + \mathbf{u}_2\cdot\nabla\right)\mathbf{u}_2 + \mathbf{e}_3\times\mathbf{u}_2 = -\nabla p_2,$$

$$\nabla\cdot\mathbf{u}_2 = \delta\left\{h_t + \nabla\cdot\left[u_2\left(h+h_B\right)\right]\right\},$$

$$p_1 = h + \sqrt{\delta}p_2,$$

where the subscripts 1 and 2 denote, respectively, upper and lower layer quantities with $\mathbf{u}_{1,2}$, $p_{1,2}$, h, and h_B the velocities, dynamic pressures, upper layer thickness, and bottom topography, respectively, and where

$$\delta = \frac{h_*}{H},$$

is the ratio of the upper layer scale thickness h_* to the lower layer scale thickness H.

Written in this form, the key asymptotic parameter is δ for which we assume $0 < \delta \ll 1$. The subinertial timescale is given by $(f\delta)^{-1}$, which is ~ 24 hours for the Gaspé region. The length scale (~ 16 km) is given by

$$L = \frac{\sqrt{g'h_*/\sqrt{\delta}}}{f},$$

where f and g' are the Coriolis parameter and reduced gravity, respectively.

The length scale is intermediate between the internal deformation radius associated with each individual layer since, assuming δ is small,

$$\frac{\sqrt{g'h_*}}{f} \ll \frac{\sqrt{g'h_*}}{\delta^{\frac{1}{4}}f} = L = \frac{\delta^{\frac{1}{4}}\sqrt{g'H}}{f} \ll \frac{\sqrt{g'H}}{f}.$$

For the Gaspé region, $\sqrt{g'h_*}/f \approx 10$ km and $\sqrt{g'H}/f \approx 27$ km. If we think of the lower layer deformation radius as a "basin" length scale, the frontal geostrophic equations can be thought of as an intermediate length scale model in the sense of *Charney and Flierl* [1981], in which the dominant nonlinearity arises not due to the advective terms in the momentum equations but rather due to density or thickness gradients in the mass or continuity equation. The scalings for the upper and lower layer velocities are given by, respectively, $\sqrt{\delta}fL \approx 55$ cm/s and $\delta fL \approx 20$ cm/s, and the dynamic pressures are scaled geostrophically. The upper layer velocity scaling is larger than the scaling for the lower layer velocity, and this results in the upper layer advective terms in the momentum equations being an order of magnitude larger than those in the lower layer momentum equations.

The model equations are derived by introducing a straightforward asymptotic expansion in powers of $\sqrt{\delta}$ into the above shallow-water equations, the details of which we do not describe here [see *Swaters*, 1993]. If the leading order upper layer frontal thickness is denoted by $h(x,y,t)$, which is also the leading order geostrophic pressure in the upper layer, and the leading order lower layer geostrophic pressure is denoted by $p(x,y,t)$, the Swaters baroclinic frontal geostrophic model can be written in the form

$$h_t + J(p + h\Delta h + \frac{1}{2}\nabla h\cdot\nabla h,\ h) = 0, \qquad (1)$$

$$(\Delta p + h)_t + J(p,\ \Delta p + h + h_B) = 0, \qquad (2)$$

where $h_B = h_B(x, y)$ is the bottom topography (see Figure 2) and

$$J(A, B) = A_x B_y - A_y B_x.$$

It is also worth pointing out that (1) and (2) correspond to the (nontrivial) leading order potential vorticity (PV) equations in each layer, respectively, in which the potential vorticity is given by $\Delta p + h + h_B$ in the lower layer and by $1/h$ in the upper layer. Alternatively, (1) can be thought of as the leading order mass conservation equation for the frontal layer in which the velocity field is determined by the leading order ageostrophic terms which arise from the upper layer momentum equations. The inclusion of these terms leads to a model which is cubically nonlinear with respect to h (see (1)). These terms correspond to the advection of frontal vorticity by the frontal flow and are necessary for instability. The reason why these advective terms are cubically nonlinear, compared to quadratically nonlinear as in QG theory, is a result of the fact that the underlying scalings used to derive (1) assume that, even at leading order, the upper layer continuity equation is fully nonlinear as a consequence of allowing for finite-amplitude thickness variations. The higher-order nonlinearity is a direct consequence of developing a model which can, in principle, describe the destabilization of fronts and the formation and evolution of eddies with genuine outcroppings [see also *Reszka and Swaters*, 1999].

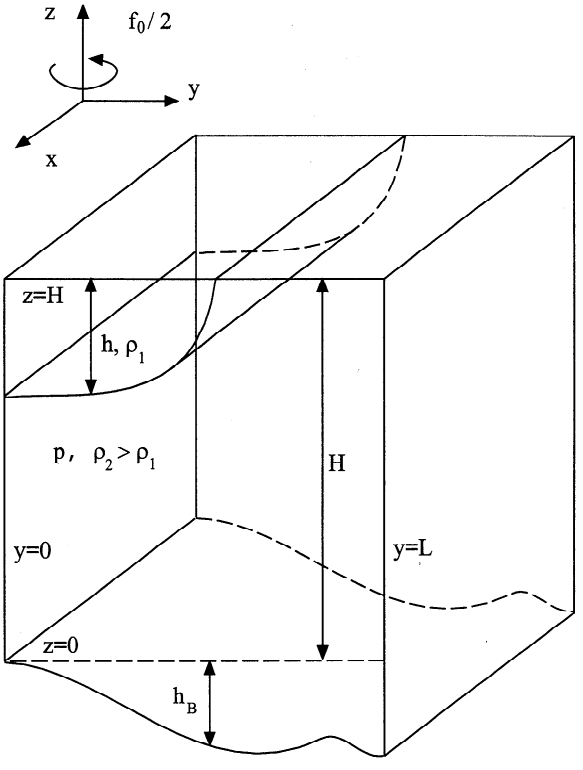

Figure 2. Model geometry associated with the governing equations. The model derivation assumes a rigid lid. While general bottom topography is allowed, our simulations employ an x-invariant bottom.

As mentioned before, this model focuses on baroclinic instability. That is to say, the barotropic limit of the model exhibits no instability whatsoever for monotonic frontal profiles [*Swaters*, 1993]. (Shear instability is allowed but only in coupled fronts.) While there is almost certainly a barotropic component to the observed instability, *Mertz et al.* [1988] assert that the baroclinic mechanism is indeed important, perhaps dominant, in the Gaspé Current. Basing their arguments on energy conversion calculations, they reach a similar conclusion with respect to the Gaspé precursor. We therefore believe that the present model describes an important aspect of the transition to instability of the flow in the NWG and LSLE.

As mentioned previously, the principal objective of this paper is to numerically simulate, using our baroclinic frontal geostrophic equations, the transition to instability for the flow in the NWG and LSLE regions and to compare the results of our simulations to observations for these regions. As we will show, the model reproduces many aspects of the transition to instability very well. The purpose of the present paper is not, however, to provide a detailed exposition of the general dynamical characteristics of numerical solutions to our frontal geostrophic equations. A discussion of this kind is presented by *Reszka and Swaters* [1999], in which a general investigation of the behavior of buoyancy-driven coastal currents based on a series of numerical experiments and analytical methods for our frontal geostrophic model is given.

Specifically, a series of simulations for isolated or upwellings fronts was described which demonstrated realistic meandering of the frontal outcropping(s), filamentation, and the development of both warm-core and cold-core eddies. *Reszka and Swaters* [1999] showed that the frontal geostrophic model can describe eddy merger, separation, or reabsorption into the background flow. Despite the assumption of only two layers, it was shown that the growth rates and length scales of the emergent features are in good agreement with results of a number of studies based on more sophisticated primitive equation models.

General simulations of coupled fronts were also described by *Reszka and Swaters* [1999]. They found that such currents break up into distinct vortices which propagate very little, but which do exhibit merging and splitting, behavior consistent with previous numerical studies involving similar models, as well as laboratory experiments.

Reszka and Swaters [1999] showed that the cross-front topographic slope has a significant effect on the instability. Indeed, it was shown that the onset of instability is due to the coalesence of barotropic and baroclinic topographic Rossby wave modes. In addition to a numerical study, *Reszka and Swaters* [1999] presented an analytical nonlinear wave packet stability theory for a marginally unstable flow. They showed that the unstable modes can saturate as solitons.

3. Numerical Scheme

For the purposes of numerical computation we put (1) and (2) into the following form:

$$h_t = J(h,\ p + h\Delta h + \frac{1}{2}\nabla h \cdot \nabla h), \tag{3}$$

$$q_t = J(q,\ p), \tag{4}$$

$$\Delta p = q - h - h_B, \tag{5}$$

where the lower layer vorticity is given by $q = \Delta p + h + h_B$.

We chose to use an explicit, finite difference algorithm that is leapfrog in time and central in space (second-order accurate in both cases). The Jacobian terms are approximated via the *Arakawa* [1966] formula, which preserves energy and enstrophy conservation and the underlying skew symmetry. A conjugate gradient technique is used to invert the Laplacian in (5) to recover the lower layer pressure at each time step. We introduced the Robert filter [*Asselin*, 1972], with a coefficient of 5.0×10^{-3}, to help suppress the computational mode. Numerical friction proportional to $\Delta^8 h$, with a coefficient of 5.0×10^{-20}, is employed in the upper layer equation (3) to eliminate small-scale noise.

The computational domain is a periodic channel given by

$$\Omega = \{(x, y) \mid 0 < x < x_{\max},\ 0 < y < L\}.$$

All flow fields are assumed to be smoothly periodic across $x = 0$, $x_{\max}$ and a no-normal-flow condition is applied on the channel walls at $y = 0$, L. That is, we employ Dirichlet boundary conditions on both geostrophic pressures, p and h, such that

$$\left.\frac{\partial h}{\partial x}\right|_{0,L} = \left.\frac{\partial p}{\partial x}\right|_{0,L} = 0.$$

Since our choice of initial conditions has $p = 0$ on $y = 0$, L at $t = 0$, the boundary values of p will be zero for all t. The boundary values of h remain fixed at their initial x-invariant values, as determined by the initial profile. In the finite differencing of (3), one is required to evaluate $h\Delta h + \nabla h \cdot \nabla h/2$ on the channel walls. This was done using one-sided, second-order accurate interior finite differences.

As the velocity shear in the NWG below ~ 40 m is very small [*Benoit et al.*, 1985], we assume there is no mean flow in the lower layer initially. We note, however, that since the model equations (1) and (2) are invariant under the Galilean-like transformation

$$p \to p - Uy, x \to x - Ut,$$

for all U, it follows, in any event, that an unsheared mean flow in the lower layer can always be mathematically removed from the governing equations by choosing an appropriate co-moving reference frame; that is, an unsheared mean flow in the lower layer has no dynamical importance other than to Doppler shift frequencies and real-valued phase velocities.

The lower layer pressure, however, was seeded with a random perturbation (whose kinetic energy, denoted by KE, was 10% of the upper layer mean KE), to initiate the instability process. No perturbation was introduced into the upper layer at $t = 0$. The instability is initiated owing to the presence of the perturbations in the lower layer. Numerical integration was carried out until the system reached a quasi steady state (between 20 and 30 days) as determined from examining the time development of the upper and lower layer perturbation energies.

Tracking of the interfacial outcropping can be problematic in numerical simulations. As shown in a detailed asymptotic analysis by *Swaters* [1993, Section 2b and equations (2.20) and (2.21)], however, in the frontal geostrophic limit associated with (1) and (2), the appropriate kinematic and dynamic boundary conditions on an outcropping reduce to (3) when evaluated on the outcropping, regardless of whether or not h smoothly vanishes. Since the upper layer equation (3) is trivially satisfied whenever $h = 0$, the location of the outcropping is determined automatically by simply integrating (3) over the entire domain. We note that whenever $h = 0$, the model equations reduce to simply (4) and (5) with $h = 0$. This is a clear advantage of the Swaters model that underscores its utility in numerical process studies related to the dynamics of outcroppings compared to, for example, primitive equation simulations.

The occurrence of negative values of h in the immediate region surrounding an undulating outcropping in our numerical simulations is an inevitable consequence of the finite difference discretization. Because negative h values are unphysical (that is, the total upper layer thickness can never be negative), after each time step we demand that $h(x, y, t) = \max\{h(x, y, t), 0\}$ for each pair of (x, y) coordinates. This procedure may be thought of as introducing a delta function type of numerical friction, acting on the grid scale itself [R. H. Karsten and G. E. Swaters, Nonlinear effects in two-layer, frontal-geostrophic dynamics, 1, The strong β case, submitted to *Journal of Fluid Mechanics*, 1999a]. Indeed, if we do not implement this procedure, our numerical integration rapidly exhibited numerical instability. The net physical effect of this procedure is to introduce a very slight increase in the area-integrated, upper layer mass throughout the integration.

While along-front variations in bottom topography are believed to trigger the onset of instability in some coastal currents [*Haidvogel et al.*, 1991], in this series of experiments we chose to focus on the effect an x-invariant bottom slope. The modeled topography consists of two half parabolas, joined by a horizontal line segment, as depicted in Figure 3 (dashed line). Dimensionally, this profile has a maximum depth of 335 m and corresponds to the actual cross-channel bottom topography (Figure 3, solid line) near Ste.-Marthe-de-Gaspé, as reported by *Benoit et al.* [1985]. While the NWG widens considerably over its entire length, the bathymetry directly beneath the jet remains more or less constant. We therefore believe the above approximation to be reasonable. It should be noted that the *Swaters* [1993] model was initially derived with the assumption that, on average, the height of the bottom topography is small in comparison to the mean depth of the lower layer. The lower layer equation (4) will therefore be dominated by the h_B term close to the shore.

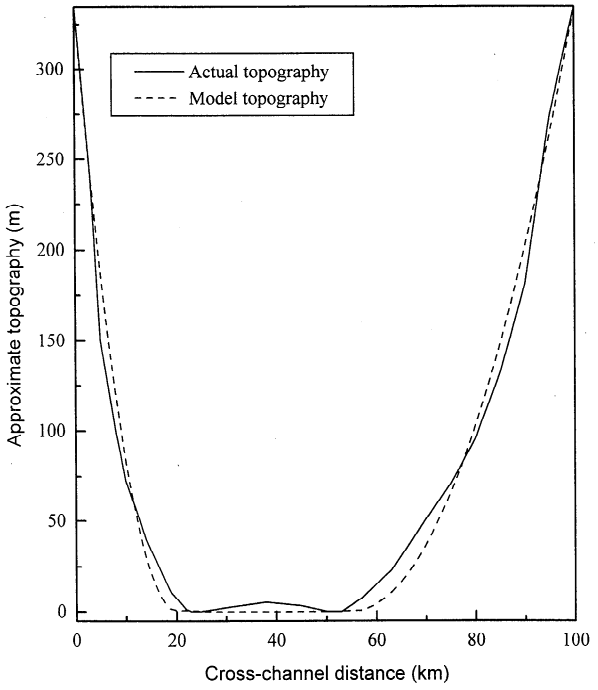

Figure 3. Cross-channel bottom topography used in model (solid line) and actual topography (dashed line) as measured near Ste.-Marthe-de-Gaspé.

4. Description of Results

4.1. Quadratic Profile

It is generally accepted that the core of the jet comprises the upper 30 m of the water column [*Mertz et al.*, 1988], which is thin compared to the total fluid depth. Since the mean depth of the NWG as well as the LSLE is between 200 and 300 m, we easily obtain a small depth ratio as our model requires. For the main experiment we defined the initial (nondimensional) frontal profile as follows:

$$h_o = \max\left[1.0 - 0.7y^2,\ 0.0\right]. \tag{6}$$

This gives a mean (dimensional) depth of 27 m and a mean along-front geostrophic velocity of 46 cm/s. The maximum velocity occurs at the outcropping ($\sim$ 18 km offshore) and has a value of 83 cm/s. Because the length of the channel greatly influences the length scale of growing instabilities, the numerical model was first executed with a channel length of 480 km, long enough for several unstable waves. It was found that the most unstable mode had a wavelength of $\sim$ 60 km, which is consistent with observations of *Tang* [1980a] concerning the Gaspé Current as well as *Mertz et al.* [1990] concerning the Gaspé precursor.

The simulation was then performed in a 120-km channel, and we present the results here. This numerical experiment will be referred to as case A. The thickness profile is plotted in Figure 4a (as the solid line) from the south shore to the outcropping, while the corresponding geostrophic velocity profile is plotted in Figure 4b (solid line). Initially, the jet developed a wave number 2 instability and the disturbance grew to finite size (roughly 20 km in the cross-channel direction) at 6 days. The phase speed was found to be $\sim$ 24 cm/s downstream, in excellent agreement with *Tang* [1980a]. The wave then decayed to a very small amplitude over the next 3 days. The growth/decay cycle occurred two more times, with maximum amplitudes observed at 11 and 16 days. *Tang*

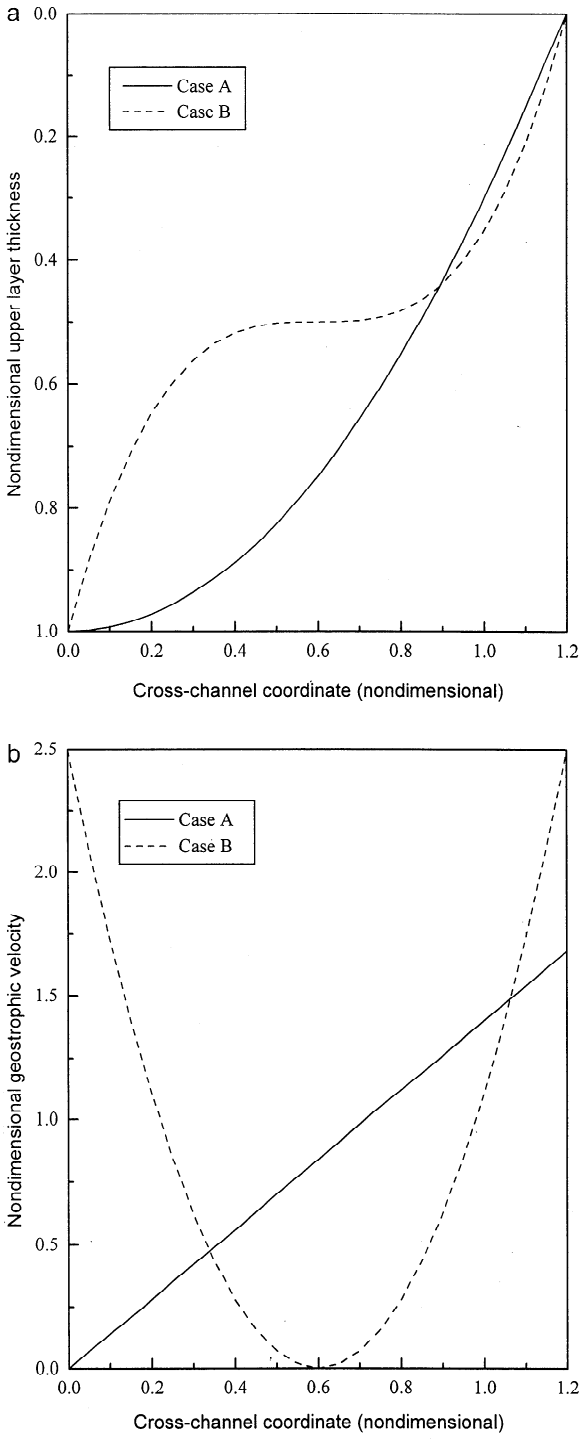

Figure 4. Initial (nondimensional) frontal height (a) and upper layer geostrophic velocity (b) profiles for case A (solid line) and case B (dashed line), respectively, plotted versus the (nondimensional) cross-channel coordinate from the south shore to the outcropping.

[1980a] has also reported the presence of waves that grow and collapse on a timescale of several days. At day 21 of the simulation the instability shifted to larger scales. A single meander developed and pinched off, forming an isolated anticyclonic eddy.

Figures 5a through 5e display contour plots of the upper layer stream function, h, at 0, 4, 6, 21, and 23 days, respectively. The contour range is 0 to 40 m, and the contour interval is 8 m. Shaded areas correspond to $h = 0$ (that is, the lower layer comprises the entire fluid column). In Figure 5a

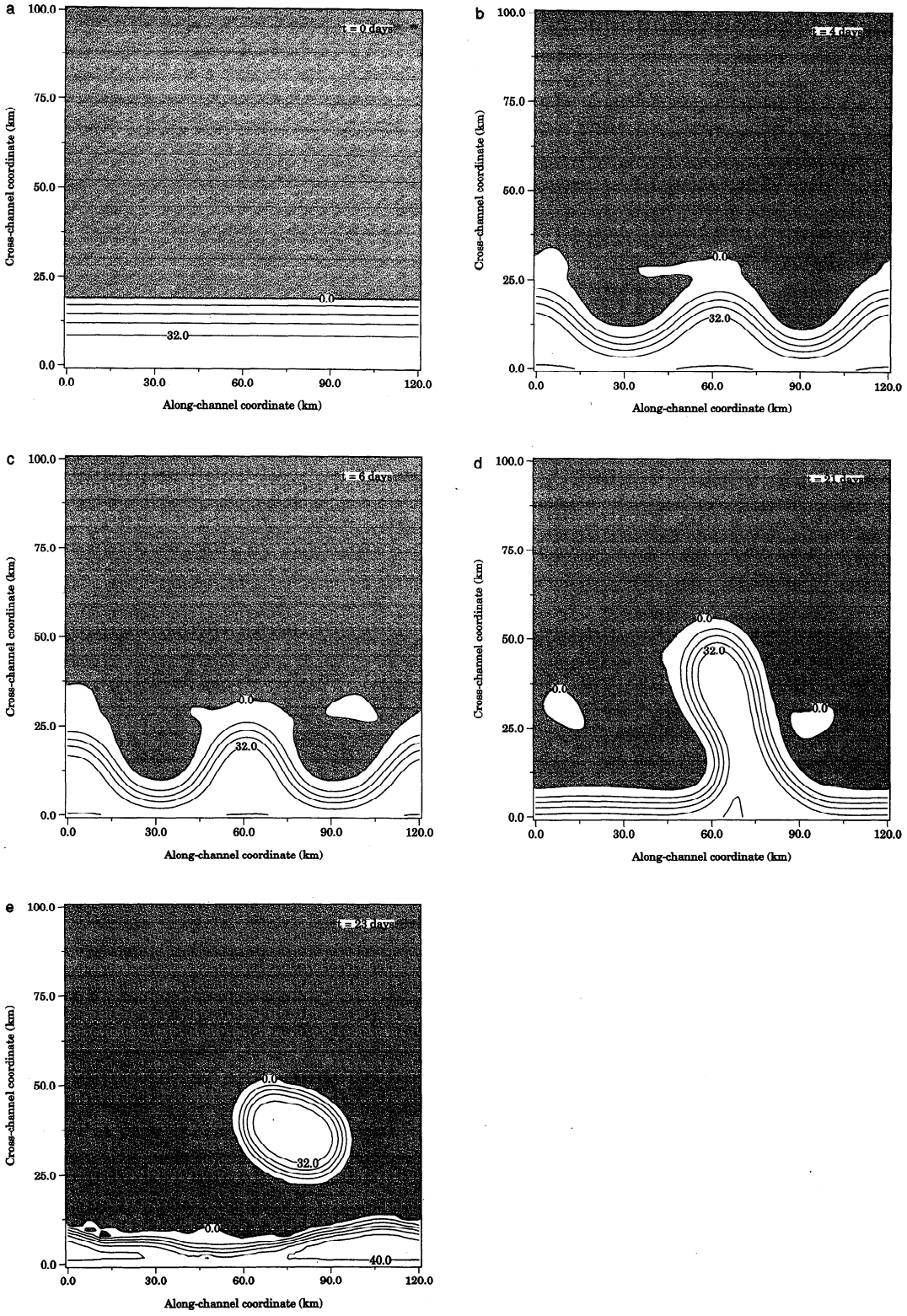

Figure 5. Case A (quadratic profile) showing dimensional upper layer streamfunction, h, at (a) 0 days, (b) 4 days, (c) 6 days, (d) 21 days, and (e) 23 days. Range and contour interval are 0 to 40 and 8 m, respectively. Shaded areas correspond to $h = 0$.

the x-invariant current lies adjacent to the south shore and the lower layer pressure consists of a small random perturbation. In Figure 5b the instability develops, growing to its maximum amplitude in Figure 5c. The front has intensified considerably and exhibits velocities of up to 1.1 m/s. During this time the lower layer pressure has organized itself into a series of alternating high-pressure and low-pressure cells, directly beneath the current. Both subsequent instability events are qualitatively similar to Figures 5b and 5c. Figure 5d shows the growing meander that later gave rise to an anticyclonic vortex. This eddy (Figure 5e) was fairly stable and remained isolated for the next several days. More will be said about upper layer eddies in the next subsection, where we describe simulations of fronts with cubic profiles.

In Figure 6 we have plotted the offshore edge of the current only, so that the shape of the frontal outcropping may be compared with the drawings in Figure 1. Figure 6 a (day 7 of the simulation) emphasizes the backward breaking phenomenon, so ubiquitous in the estuarine/gulf system. Figure 6b (day 18) shows a single wave with two slender streamers extending backward from the wave crest, not unlike the August 5th image in Figure 1.

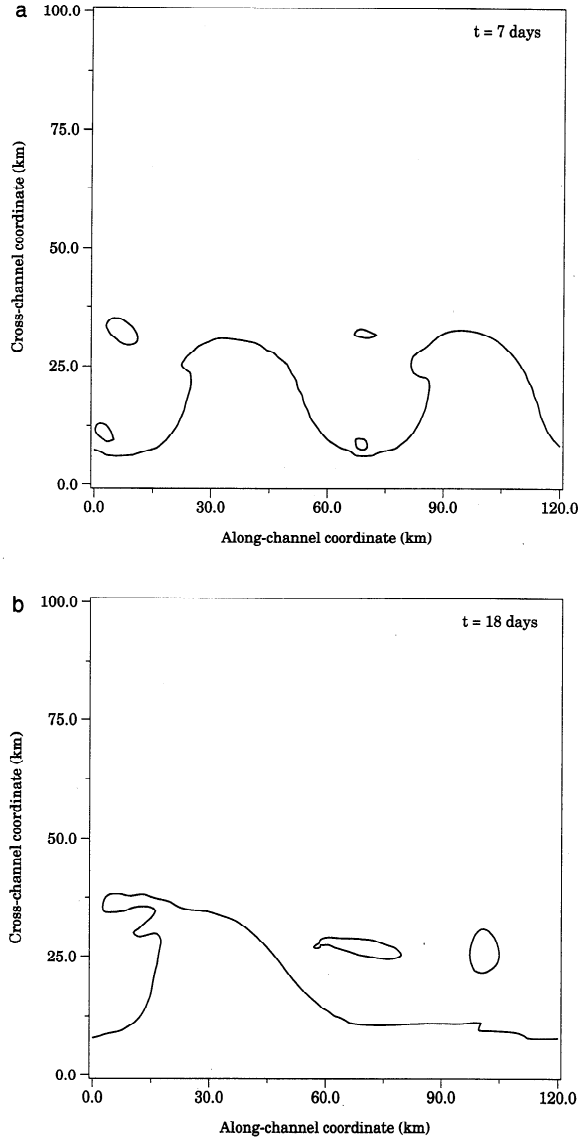

Figure 6. Outcropping (i.e., edge of current) at (a) 7 days and (b) 18 days of the simulation for case A. Backward breaking of the wave is visible in (a) and two streamers are seen to emanate from the crest of the wave in (b).

We estimate e-folding times of ~ 4 days. While this compares reasonably well with the timescales observed by *Tang* [1980a], it must be noted that *Mertz et al.* [1988] suggest an e-folding time of 7 days in association with an instability event in the summer of 1985. The time-averaged volume flux for days 0 to 23 of the simulation was found to be 1.85×10^5 m$^3/s$ (eastward). For comparison, *Benoit et al.* [1985] estimated the instantaneous net geostrophic transport for the upper 30 m in June of 1978 to be $\sim 1.36 \times 10^5$ m^3/s. They emphasize, however, that large deviations in volume transport are not uncommon. The theoretical (time invariant) volume flux for the model can be computed using the initial condition alone and has a value of 1.77×10^5 m^3/s. The discrepancy between the theoretical value and the simulation result is due to a small but appreciable increase in upper layer mass, which we attribute to numerical friction.

The above mentioned eddy had a maximum diameter of 45 km. An anticyclonic vortex of similar size is known to develop near the mouth of the LSLE during the summer months [*El-Sabh and Silverberg*, 1990]. Cyclonic eddies in the LSLE and NWG have been reported by *Mertz et al.* [1988, 1990], and others. (A particularly striking satellite image appears in the work by *Mertz et al.* [1990].) In the laboratory experiments of *Griffiths and Linden* [1982], regions of cyclonic vorticity were seen to form behind the wave crests of an unstable surface current, leading to "backward breaking" waves. In our two-layer model the region behind each wave crest is composed mostly, or entirely, of lower layer fluid. In Figures 7a-7d we have plotted the lower layer stream function at 0, 4, 6, and 21 days, respectively, i.e., corresponding to Figure 5. Examining the lower layer pressure, we see cyclonic cells at day 4, located directly behind the wave crests of the upper layer in Figure 5b. (See also the backward breaking effect in Figure 6).

It is noteworthy that these low-pressure cells are considerably stronger than the adjacent high-pressure cells. The cyclonic vortices intensify at day 6 and weaken over the next 3 days. The strength of the vortices peaks two more times, at day 11 and day 16, i.e., in phase with the frontal instability modulation described previously. Finally a rather strong cyclonic gyre develops by day 21, at which point the maximum lower layer velocity is ~ 45 cm/s.

4.2. Cubic Profile

While the quadratic function in (6) is a reasonable approximation for the initial frontal profile, some σ_t sections in (for example) the work by *Benoit et al.* [1985] show several isopycnals in the upper 50 m which are steep at the coast, then level off, then steepen again in the vicinity of the outcropping. This suggests a cubic-like initial profile for the upper layer, which results in a double maximum in the

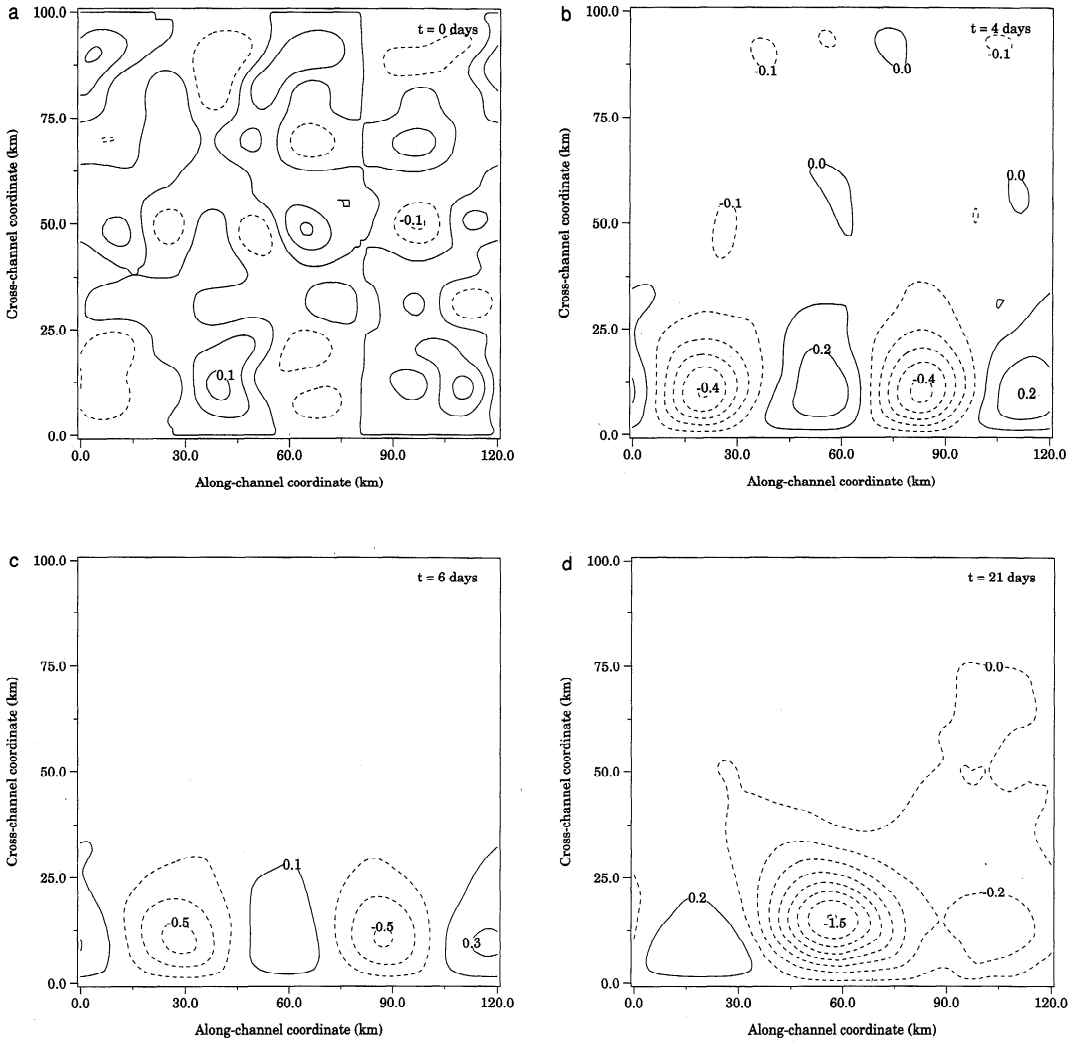

Figure 7. Case A showing nondimensional lower layer streamfunction p at (a) 0 days, (b) 4 days, (c) 6 days, and (d) 21 days. Range and contour interval are (a) -0.1 to 0.1 and 0.05, (b) -0.4 to 0.2 and 0.1, (c) -0.5 to 0.3 and 0.2, (d) -1.5 to 0.3 and 0.2.

geostrophic velocity. Presumably, such isopycnal configurations are more prevalent during high run-off conditions, when the current spreads in the offshore direction, a process which sometimes precedes an instability event [*Tang*, 1980a]. We note that the ongoing instability in CASE A did not yield such a thickness profile, and it therefore warrants its own investigation.

In this subsection we describe a simulation with h_o defined nondimensionally as follows:

$$h_o = \max\left[0.5 - 2.31(y - 0.6)^3,\ 0.0\right]. \qquad (7)$$

The front cross section is plotted as the dashed line in Figure 4a, while the corresponding geostrophic velocity profile is the dashed line in Figure 4b. The above definition results in a current $\sim$ 20 km wide, with a mean depth of 21 m. Maximum velocities are to be found at the channel boundary as well as the outcropping, and the velocity vanishes half way across the front. The mean and maximum velocities are 55 and 134 cm/s, respectively. Again, the governing equations were first integrated in a 480-km channel, until a dominant wavelength could be discerned. This wavelength was found to be 60 km, and a detailed simulation (called case B) was then performed in a 120-km channel, the results of which are presented below. The channel geometry was the same as in case A, and an initial perturbation at the 10% level was again imposed on the lower layer stream function p.

The first stage of the instability progressed similarly to case A. The front deformed into two waves which grew and were then modulated over $\sim$ 20 days. Backward breaking frontal waves and lower layer cyclonic cells could be observed, but were not as pronounced as in Case A. The frontal region became narrow, exhibiting geostrophic velocities of up to 1.3 m/s.

An anticyclonic eddy separated from the front at 25 days, and several interesting developments occurred over the next few days. Figures 8a-8d shows the upper layer stream function at 26, 27, 28, and 29 days, respectively. The contour range and interval are the same as in Figure 5 and, again, areas where $h = 0$ are shaded. Between days 26 and 27

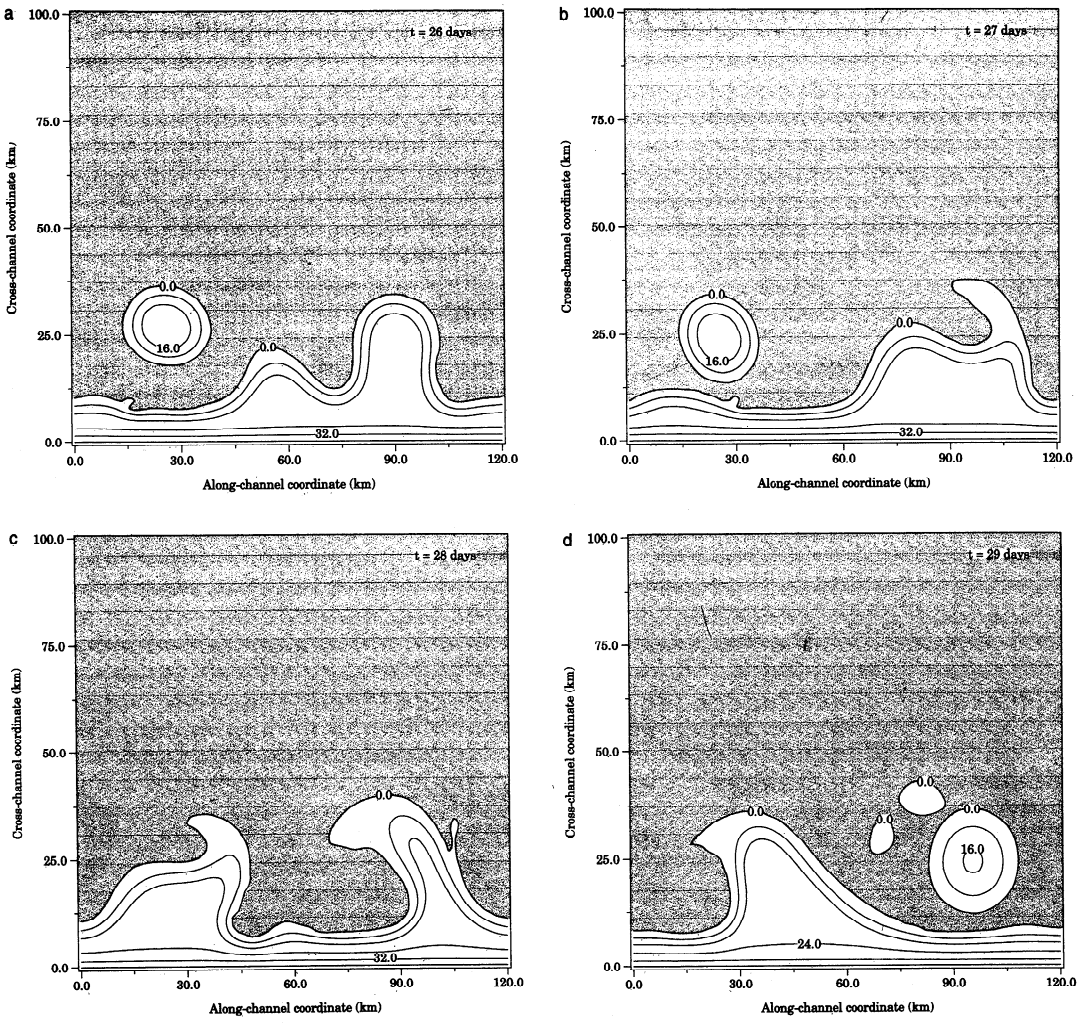

Figure 8. Case B (cubic profile) showing dimensional upper layer streamfunction, h, at (a) 26 days, (b) 27 days, (c) 28 days, and (d) 29 days. Range and contour interval are 0 to 40 and 8 m, respectively. Shaded areas correspond to $h = 0$.

the wave that gave rise to the eddy merged with the neighboring wave, and their interaction caused a small filament to protrude in the offshore direction (Figure 8b). The existing eddy was reabsorbed, and two cross-shore protrusions can be seen in Figure 8c, which should be compared with the August 7 and August 8 images of the Gaspé Current in Figure 1. Finally, a new eddy pinched off at day 29 (Figure 8d). Overall, the cubic frontal profile was found to be more conducive to eddy pinch-off, filament growth, and eddy-mean-flow interaction. This is not surprising, as the offshore half of the current was more shallow in case B than case A.

Both vortices that appeared in the above simulation had a diameter of roughly 25 km and a maximum depth of 20 m. Upper layer eddy features obtained with this model are typically elliptical in shape, and a clockwise rotation of the major axis is superimposed upon the clockwise motion of the fluid within the eddy [*Reszka and Swaters*, 1999]. As was mentioned previously, the instability process we are investigating depends on the baroclinic mechanism. Figure 9 demonstrates the release of available potential energy (APE) stored in the sloping interface for the above simulation. The APE is defined as

$$\frac{1}{2} g \Delta\rho \iint_{\Omega} (h - h_{\text{ref}})^2 dx dy, \tag{8}$$

[*Cushman-Roisin*, 1994], where h_{ref} is the thickness of a rectangular slab whose volume is exactly that of the upper layer. (Given the profile (7), $h_{\text{ref}} \approx 0.095$). We compute (8) from the model output at 2-hour intervals, and the resulting values (normalized by the initial APE) are plotted for the first 30 days of the simulation. We remark that a thorough discussion of the analytical and numerical aspects of baroclinic energy release in this and other frontal models is given by R. H. Karsten and G. E. Swaters (Nonlinear effects in two-layer, frontal-geostrophic dynamics, 1, The strong β case, submitted to *Journal of Fluid Mechanics*, 1999a; Nonlinear effects in two-layer, frontal-geostrophic dynamics, 1,

The weak β case, submitted to *Journal of Fluid Mechanics*, 1999b).

Though not monotonic, a general decreasing trend is easily discerned in the APE curve (Figure 9). For the first few days the lower layer disturbance initiates a similar perturbation in the upper layer. The first significant drop in APE occurs at $\sim$ 7 days, when the outcropping first deforms. The deformation amplitude decays, then grows again, forming backward breaking waves, at which point the APE decays significantly once more (19 days). The shedding of an anticyclonic eddy at 26 days causes a loss of APE, which is quickly regained when the eddy reattaches to the current. When another eddy separates at 30 days, the APE decays once more. At this point the APE has lost $\sim$ 25% of its original value. Presumably, the current might undergo further instability, releasing more of the potential energy. It is unlikely, however, that this process would go on until all of the APE was extracted, since the requirement that h be kept constant on the inshore boundary eliminates the possibility that the upper layer could flatten out completely. In either event, we did not pursue this question further, as the instabilities observed in the Gaspé Current are typically modified by changing external factors on timescales shorter than a month.

4.3. Effect of Topography

A series of simulations was performed in order to elucidate the role of bottom topography on the instability process. The flow configuration was exactly the same as in case A, but the bathymetry amplitude was scaled by a parameter that ranged between 0 and 1. The following four scenarios were examined: a flat bottom, small bottom topography (of the order of the upper layer thickness), half-height topography, and normal topography (i.e., exactly the amplitude used in case A and B). The lower layer KE was tracked over the next 4 days, and the results are plotted in Figure 10. We note that the lower layer KE is a good indicator of the overall growth of the instability, since the lower layer pressure consists entirely of the growing perturbation.

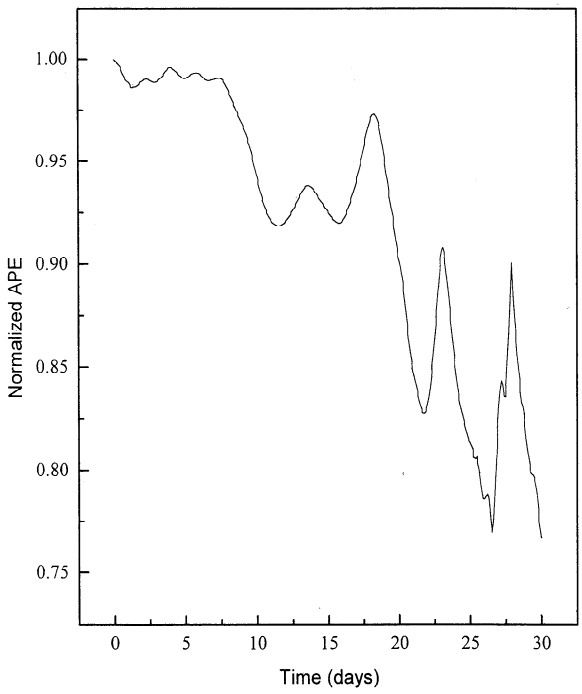

Figure 9. Normalized avialable potential energy versus time (days) for the case B simulation. The general decreasing trend underscores the process of baroclinic energy release.

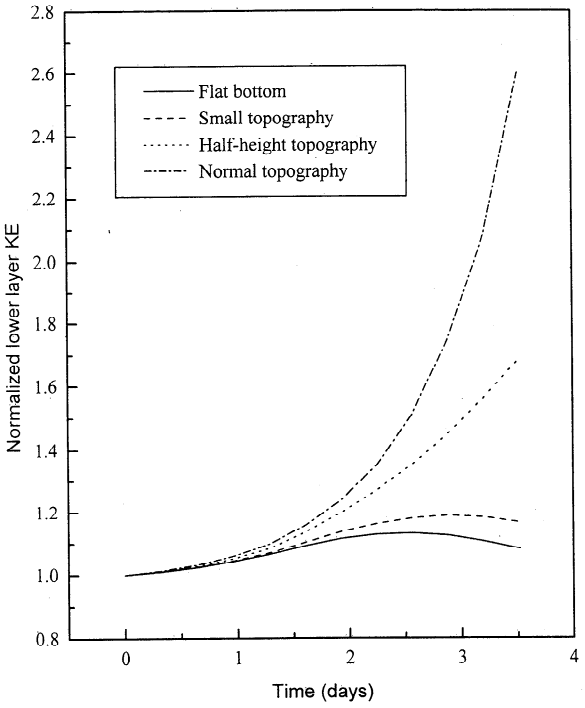

Figure 10. Normalized lower layer kinetic energy versus time (days) for four different scalings of the bottom topography.

Clearly, with a flat bottom, the instability is very weak. It reaches its maximum amplitude at $\sim$ 2.5 days and is then modulated. When topography is small (compared with the channel depth), growth is slightly more pronounced. With half-height and normal-height topography the growth rate increases further (these instabilities are also modulated but at longer times). This study indicates therefore that the bathymetry existing in the NWG is instrumental in the onset of instability events in the Gaspé Current.

It must be stressed that because the bottom topography underneath the current slopes in the opposite sense to the frontal interface, the effect of topography is a destabilizing one, which is at variance with an assertion made by *Tang* [1980a]. The gradients of isopycnals associated with offshore currents, such as the upwelling front off the coast of Oregon [e.g., *Barth*, 1989], are often of the same sign as the cross-front topographic gradients. Previous modeling results show that in such a case, the bottom slope can decrease the perturbation growth rate or, indeed, eliminate instability al-

together (see *Orlanski* [1969], *Mechoso and Sinton* [1981], and others). Indeed, the situation is analogous to the effect of the β plane on eastward and westward flowing currents.

It is quite likely that, owing to continuous stratification of the water column, the Gaspé Current is "cushioned" or "isolated" somewhat from the effects of the bottom slope. Since the topography is a destabilizing force, the net result is to decrease the growth rate. Indeed, this may be a reason why e-folding times associated with the Gaspé Current are (at least sometimes) slightly longer than the ones we have reported. In the model by *Swaters* [1993], the lower layer directly transmits information from the bottom to the upper layer. As such, it may overestimate the importance of bottom topography to some degree.

5. Conclusions

Numerical solutions relevant for the Gaspé Current have been presented, using a model that focuses on baroclinic dynamics. Our simulations describe both the initial growth of the instability, as well as later stages of frontal evolution, including such highly nonlinear processes as eddy pinch-off and reabsorption. On the basis of observation, quadratic and cubic frontal thickness profiles were investigated, and it was found that the spatial and temporal characteristics of the instability are generally in agreement with observations. Disturbances exhibit a dominant length scale of $\sim$ 60 km and e-folding times of 4-5 days, with a downstream propagation speed of $\sim$ 20 cm/s. The existence of backward breaking waves, and cyclonic and anticyclonic eddies also compares favorably with previous observational studies. We point out that even though the present model incorporates only two layers, it is an isopycnic model and therefore fully describes the three-dimensional structure of the upper layer, where the current exists.

The effect of the bottom topography was examined by scaling the topography and tracking the perturbation growth. It was found that with small (or flat) bottom topography the instability is very weak. It seems therefore that the steep topography present in the NWG has a crucial (destabilizing) effect on the growth rate. The present study did not include an investigation of the effects of topographic variations in the along-channel direction. Future work should determine what, if any, influence such variations may have on the onset of instability.

Acknowledgments. Preparation of this manuscript was supported in part by a research grant awarded by the Natural Sciences and Engineering Research Council (NSERC) of Canada and by science subventions awarded by the Department of Fisheries and Oceans of Canada and the Atmospheric Environment Service of Canada to G.E.S. and by a NSERC Postgraduate Scholarship and a Graduate Teaching Assistantship awarded to M.K.R.

This paper is dedicated to the memory of Tertia M.C. Hughes.

References

Arakawa, A., Computational design for long-term numerical integration of the equations of fluid motion: Two-dimensional incompressible flow, 1, *J. Comput. Phys., 1*, 119-143, 1966.

Asselin, R. A., Frequency filters for time integrations, *Mon. Weather Rev., 100*, 487-490, 1972.

Barth, J. A., Stability of a coastal upwelling front, 1, Model development and a stability theorem, *J. Geophys. Res., 94*, 10,844-10,856, 1989.

Benoit, J., M. I. El-Sabh, and C. L. Tang, Structure and seasonal characteristics of the Gaspé Current, *J. Geophys. Res., 90*, 3225-3236, 1985.

Charney, J. G., and G. R. Flierl, Oceanic analogues of large-scale atmospheric motion, in *Evolution of Physical Oceanography - Scientific Surveys in Honor of Henry Stommel*, edited by B. A. Warren and C. Wunsch, pp. 504-548, MIT Press, Cambridge, Mass., 1981.

Cushman-Roisin, B., Frontal geostrophic dynamics, *J. Phys. Oceanogr., 16*, 117-127, 1986.

Cushman-Roisin, B., *Introduction to Geophysical Fluid Dynamics*, Prentice-Hall, Englewood Cliffs, N.J., 1994.

Cushman-Roisin, B., G. G. Sutyrin, and B. Tang, Two-layer geostrophic dynamics,1, Governing equations, *J. Phys. Oceanogr., 22*, 132-143, 1992.

El-Sabh, M. I., and N. Silverberg (Eds.), *Oceanography of a Large-Scale Estuarine System. The St. Lawrence*, Springer-Verlag, New York, 1990.

Griffiths, R. W., and P. F. Linden, The stability of buoyancy-driven coastal currents, *Dyn. Atmos. Oceans, 5*, 281-306, 1981.

Griffiths, R. W., and P. F. Linden, Laboratory experiments on fronts, *Geophys. Astrophys. Fluid Dyn., 19*, 159-187, 1982.

Haidvogel, D. B., A. Beckmann, and K. S. Hedström, Dynamical simulations of filament formation and evolution in the coastal transition zone, *J. Geophys. Res., 96*, 15,017-15,040, 1991.

Karsten, R. H., and G. E. Swaters, A note on the stability theory of buoyancy-driven ocean currents over a sloping bottom, *Z. angew Math. Phys., 47*, 28-38, 1996.

Mechoso, C. R., and D. M. Sinton, Instability of baroclinic flows with horizontal shear along topography, *J. Phys. Oceanogr., 11*, 813-821, 1981.

Mertz, G., and M. I. El-Sabh, An autumn instability event in the Gaspé Current, *J. Phys. Oceanogr., 19*, 148-156, 1989.

Mertz, G., M. I. El-Sabh, D. Proulx, and A. R. Condal, Instability of a buoyancy-driven coastal jet: The Gaspé Current and its St. Lawrence precursor, *J. Geophys. Res., 93*, 6885-6893, 1988.

Mertz, G., Y. Gratton, and J. A. Gagné, Properties of unstable waves in the St. Lawrence Estuary, *Atmos. Ocean., 28*, 230-240, 1990.

Orlanski, I., The influence of bottom topography on the stability of jets in a baroclinic fluid, *J. Atmos. Sci., 26*, 1216-1232, 1969.

Reszka, M. K., and G. E. Swaters, Eddy formation and interaction in a baroclinic frontal geostrophic model, *J. Phys. Oceanogr.*, in press, 1999.

Swaters, G. E., On the baroclinic dynamics, Hamiltonian formulation, and general stability characteristics of density-driven surface currents and fronts over a sloping continental shelf, *Philos. Trans. R. Soc. London Ser. A, A345*, 295-325, 1993.

Tang, C. L., Observation of wave-like motion of the Gaspé Current, *J. Phys. Oceanogr., 10*, 853-860, 1980a.

Tang, C. L., Mixing and circulation in the northwestern Gulf of St. Lawrence: A study of a buoyancy–driven system, *J. Geophys. Res., 85*, 2787-2796, 1980b.

M. K. Reszka and G. E. Swaters, Department of Mathematical Sciences, University of Alberta, Edmonton, Alberta, Canada, T6G 2G1. (mreszka@parabolic.math.ualberta.ca; gordon.swaters@ualberta.ca)

(Received September 14, 1998; revised May 7, 1999; accepted June 30, 1999.)